

Enhanced piezoelectricity and electronic band structure transition assisted by atomic shift in MoS₂ monolayer

Sheng Yu*, Quinton Rice, Tikaram Neupane, Bagher Tabibi and Felix Jaetae Seo

*Advanced Center for Laser Science and Spectroscopy, Department of Physics, Hampton University, Hampton, VA 23668, USA, *sheng.yu@hamptonu.edu*

Abstract

Piezoelectricity appears in the inversion asymmetric crystal that converts mechanical deformational force to electricity. Two-dimensional transition metal dichalcogenide (TMDC) monolayers exhibit the piezoelectric effect due to the inversion asymmetry. The intrinsic piezoelectric coefficient (e_{11}) of MoS₂ is ~298 pC/m. For the single atomic shift of Mo of 20% along the armchair direction, the piezoelectric coefficient (e_{11}) of MoS₂ with 5x5 unit cells was enhanced up to 18%, and significantly modified the band structure. The single atomic shift in the MoS₂ monolayer also induced new energy levels inside the forbidden bandgap. The defect-induced energy levels for a Mo atom shift along the armchair direction are relatively deeper than the energy levels for a S atom shift along the same direction. It indicates that the piezoelectricity and band structure of MoS₂ can be engineered by a single atomic shift in the monolayer with multi unit cells for mechano-electrical applications.

I. INTRODUCTION

Mechanical energy is one of the most ubiquitous energy sources in the environment and can be converted to electrical energy. The piezoelectricity is associated with the electric polarization changes at the ground state due to mechanical deformation. Therefore, piezoelectricity is an immediate, and stand-alone power source for charging batteries and electronic devices.¹ Recently, one- or two-dimensional materials have been considered for piezoelectric devices that harvest vibrational mechanical energy, because they are relatively sensitive to the environment and show high conversion efficiency with cost effectiveness. In addition, the atomic shift in the supercell enhances the piezoelectricity and may introduce defect-mediated energy levels.¹⁻³

The piezoelectric properties of nanowires, such as ZnO, GaN, and BN, have been studied for potential applications including sensors, transducers, and electronics.⁴⁻⁷ Power generators based on piezoelectric nanostructures have been introduced.⁸⁻¹¹ The piezoelectric conversion efficiency

of one-dimensional (1D) ZnO nanowires (NWs) was reported from 17% to 30%.¹² However, the directional alignment of 1D ZnO NWs is difficult to further advance applications in nano electromechanical systems (NEMS).¹³⁻¹⁵ In two-dimensional (2D) layered materials including hexagonal boron nitride (h-BN) and transition metal dichalcogenides (TMDCs), the orientation of the crystal layer is critical for piezo-electronic applications¹⁶⁻²⁰ including muscle dynamics and arterial repetition regulators.²¹⁻²³ A unit cell of 2D h-BN and TMDC atomic monolayers have inversion asymmetry along the armchair direction, but not along the zigzag direction.²⁴ However, the atomic shift in a supercell of monolayers creates the inversion asymmetry that may modify the piezoelectricity and energy band structure.

The piezoelectric properties of the MoS₂ monolayer have been explored experimentally as well.²⁵⁻²⁷ An open-circuit voltage for 0.53% strain along the armchair direction in a MoS₂ monolayer was reported to be 18 mV with the piezoelectric device dimension of 10 μm in length and 5 μm in width.^{26,27} The measurement and modification of the piezoresistivity of MoS₂ have been performed, indicating 2 orders of magnitude higher than graphene.^{28,29} It suggests a systematic study of piezoelectricity and band structure of atomic layers of multi unit cells with a single atomic shift along the armchair or zigzag direction in the MoS₂ monolayer, as a representation of TMDCs, is necessary to find the enhancement of piezoelectricity and band structure modification. The atomic shift includes Mo or S along the armchair or zigzag direction with fractional percentage of the atomic lattice distance. Therefore, this analysis provides formidable information of piezoelectric properties and band structure modification in response to a single atomic shift in a MoS₂ monolayer of 5x5 unit cells. The hexagonal lattice structure with D_{3h} point group has the piezoelectric tensor with components of $e_{11} = -e_{12} = -\frac{e_{26}}{2}$.³⁰ The piezoelectric coefficient of e_{21} and e_{22} may be arisen due to the atomic shift. However, this manuscript is focused on the polarization change along the armchair direction, not the zigzag direction. Therefore, this manuscript is focused on the change of piezoelectric coefficient of e_{11} due to the atomic shift.

II. METHODOLOGY

The characterizations of piezoelectric coefficient and electronic band structure of defect-mediated a MoS₂ monolayer were calculated by using first principle calculations with the

Atomistix ToolKit (ATK) package of Virtual Nanolab with density functional theory (DFT).³¹ The localized density approximation (LDA) exchange correlation with a double zeta polarized (DZP) basis was used with a mesh cut-off energy of 150 Ry.³² The electronic temperature was 300 K for all calculations. The atomic positions and lattice parameters were optimized by using the generalized gradient approximations (GGA) with the maximum Hellmann-Feynman forces of 0.05 eV/Å, which is sufficient to obtain relaxed structures.³³ The Pulay-mixer algorithm was employed as the iteration control parameter with a tolerance value of 10^{-5} .³⁴ The maximum number of fully self-consistent field (SCF) iteration steps was 1000.³² The periodic boundary condition was employed along all three directions in the hexagonal lattice.³⁵ while the distance between neighboring monolayer structures was set to be 30 Å to minimize the interaction between them, and to accurately approximate the characteristic piezoelectricity and energy band structure of the monolayer. The self-consistent field calculations were performed to guarantee full convergence within the iteration steps.

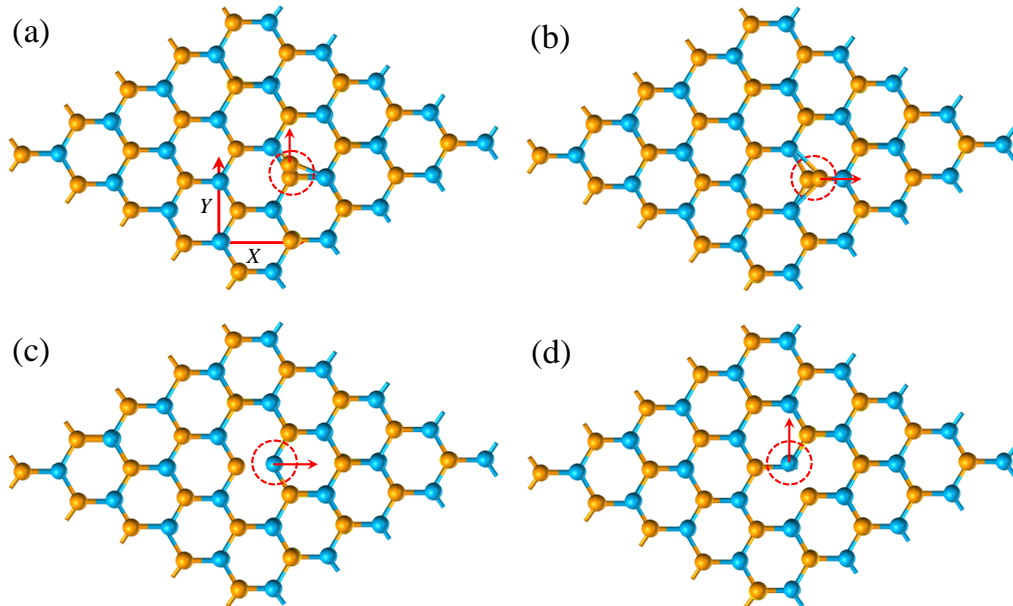


Figure 1. The schematic sketch of defect-mediated MoS₂ monolayer: (a) a single S-atom shift along positive zigzag direction, (b) a single S-atom shift along positive armchair direction, (c) a single Mo-atom shift along positive armchair direction, (d) a single Mo-atom shift along positive zigzag direction. The orange and blue spheres denote Sulfur and Molybdenum atoms, respectively. The red dot circle highlights the defect position and the red arrow indicates the atomic shift direction. X and Y denote the armchair and zigzag directions.

Figure 1 shows the schematic sketches of atomic defects in the MoS₂ monolayer. The atomic defects include S- or Mo-shift along the armchair or zigzag direction at fractional percentages of the lattice constants. One unit cell of the hexagonal lattice consists of 2 Sulfur atoms and 1

Molybdenum atom. A supercell of 5x5 unit cells includes a defect density of 1/50 for Sulfur and 1/25 for Molybdenum. The intrinsic lattice parameters of a MoS₂ monolayer without defect are 3.16 Å along the zigzag direction \vec{L}_x and 5.47 Å along the armchair direction. The atomic shift vectors in the lattice parameter \vec{L}_x and \vec{L}_y are defined along armchair and zigzag directions, respectively. The positive (negative) shift vector is along positive (negative) X- or Y-axis in Cartesian coordinate system. The unit cell along the zigzag direction \vec{L}_y has inversion symmetry, but the unit cell along the armchair direction \vec{L}_x has inversion asymmetry. The direct bandgap of MoS₂ without any defects is 1.82 eV at the K point with high symmetry in the first Brillouin zone. The piezoelectric coefficient e_{11} , is defined as the polarization gradient along the armchair direction over strain variation.²¹ The intrinsic piezoelectricity e_{11} of the MoS₂ monolayer was estimated to be ~298 pC/m, which is very close to the experimental result of 290 pC/m.³⁶ However, the piezoelectric coefficient e_{11} of the MoS₂ monolayer may be modified with atomic shifts in the supercell.

III. RESULTS AND DISCUSSION

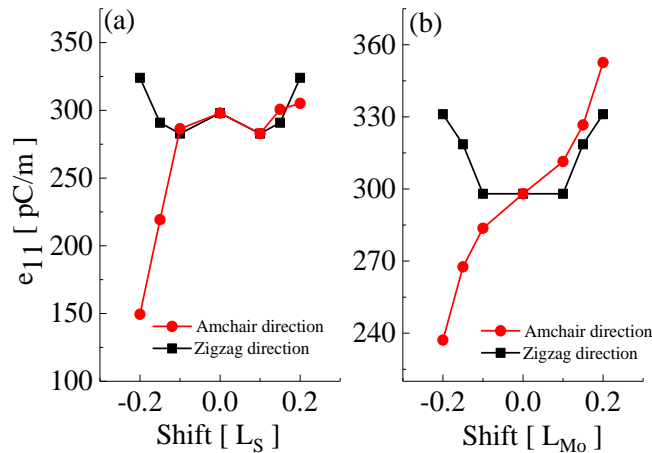


Figure 2. The evolution of piezoelectric coefficient e_{11} with (a) S shift vector and (b) Mo shift vector.

The strain-induced polarization is proportional to the piezoelectric coefficient e_{11} . Figure 2 shows the modification of the piezoelectric coefficient e_{11} due to (a) a single S atomic shift vector along the armchair and zigzag directions, and (b) a single Mo atomic shift vector along armchair direction and zigzag directions with negative or positive fractional percentage of the lattice

constant as shown in figure 1. As both S and Mo atoms were shifted along the zigzag direction, the piezoelectric coefficient e_{11} was decreased due to the electronic polarization contribution, however the coefficient was increased due to the ionic polarization contribution. Meanwhile, the piezoelectric coefficient e_{11} was almost monotonically decreased (increased) from negative to positive atomic shifts of S and Mo along the armchair direction due to electronic (ionic) polarization contributions. It indicates that the single atomic shift in the 5x5 unit cells of MoS₂ changes the piezoelectric coefficient e_{11} because the single atomic shift results in the structure modification of the supercell. It implies that the strain-induced polarization is susceptible to the electronic (ionic) charge distributions by the fractional percentage shift of Mo or S atom along the armchair or zigzag direction.

The physical origin of piezoelectricity is associated with the electric polarization changes at the ground state due to mechanical deformation.^{30,37,38} The deformation in the crystal results in the displacement of positive and negative charge centers. The charge displacement changes the electric polarization. The electronic and ionic polarization changes to the piezoelectricity are resolved by the modern theory of polarization.³⁷ The ionic contribution (P_i) to the piezoelectricity is described a simple classical electrostatic sum of point charges:

$$P_i \equiv \frac{|e|}{A} \sum_v Z_{ion}^j r^j \quad (1)$$

where Z_{ion}^j and r^j are the valence charge and position vector of atom j , A is the unit cell area, and the sum runs over all ions in the unit cell. The electronic contribution (P_e) to the polarization is obtained as:³⁷

$$P_e = -\frac{2|e|\hbar}{(2\pi)^3} \int_A dk_{\perp} \sum_{n=1}^M \int_0^{G_{\parallel}} \langle u_{n,k} | \frac{\partial}{\partial k_{\parallel}} | u_{n,k} \rangle dk_{\parallel} \quad (2)$$

where the sum runs over occupied bands, and where A is the unit cell area, M is the number of occupied bands, k_{\parallel} and k_{\perp} are parallel to and vertical to the direction of polarization, respectively. G_{\parallel} is a reciprocal lattice vector in the same direction. $|u_{n,k}\rangle$ is the cell-periodic parts of the Bloch functions, $\varphi_{n,k}(r) = u_{n,k}(r)e^{ik \cdot r}$. The last integral is the *Berry phase*. Figure 3 shows the total piezoelectric coefficient e_{11} from both electronic and ionic polarization contributions. The piezoelectric coefficient e_{11} was increased up to ~ 353 pC/m for the 20% atomic shift of Mo along the positive armchair direction, but it was significantly reduced for the atomic shift of Mo or S

atom along the negative armchair direction. For the negative or positive shift along the zigzag direction of Mo or S atom, the piezoelectric coefficient e_{11} was moderately increased.

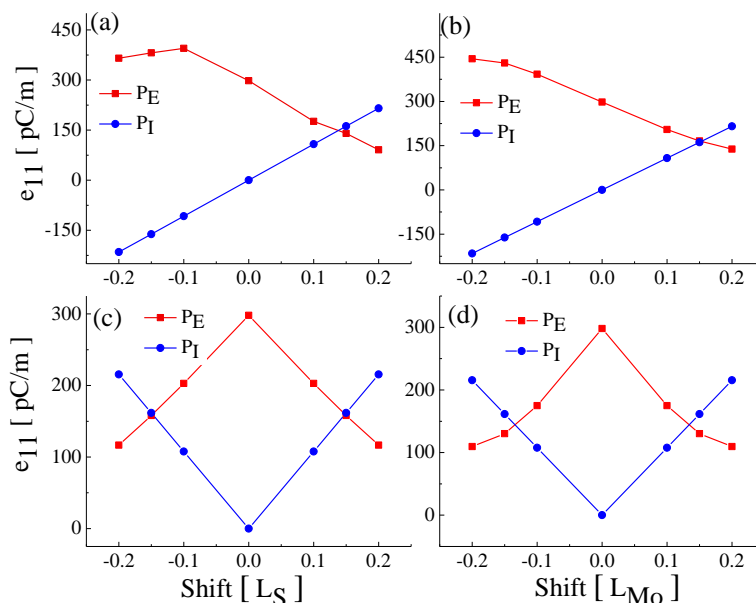


Figure 3. Evolution of piezoelectric coefficient (e_{11}) of MoS_2 due to electronic (P_E) and ionic (P_I) polarizations for the S (a) and Mo (b) atomic shift vector along armchair direction, and S (c) and Mo (d) atomic shift vector along zigzag direction.

The diverse defects of atomic vacancies, antisites, adatoms, interstitials of bulk and monolayer MoS_2 in aspects of their energy states within the forbidden band have been reported.^{39,40} The single atomic shifts of Mo and S in the 5×5 unit cells also modified the energy bandstructure of MoS_2 as shown in Figure 4. The calculation on atomic-resolved density of states was performed to distinguish the defect-induced energy levels with conduction band and valence band. The relative position of conduction band minimum (CBM) and valence band maximum (VBM) is modulated by the defects corresponding to different atomic shift length and direction. The Fermi level is close to the CBM for the S atomic shifts for figure 4 (a), (c), (d), and (f); and is close to the VBM for the Mo atomic shifts for figure 4 (g) and (j). The defect- (atomic shift-) induced energy levels apparently appeared inside the forbidden bandgap. Mo shift-induced energy levels are much deeper in the gap than S shift-induced energy levels. A S shift ($0.2 \vec{L}_X$ and $-0.2 \vec{L}_X$) along the armchair direction induced the deeper defect energy levels than a S shift along the zigzag direction ($0.2 \vec{L}_Y$). A Mo shift along the armchair and zigzag directions also shows the defect-induced energy levels close to the Fermi level. In general, the larger shift of single atom Mo or S induces

the deeper defect energy levels.

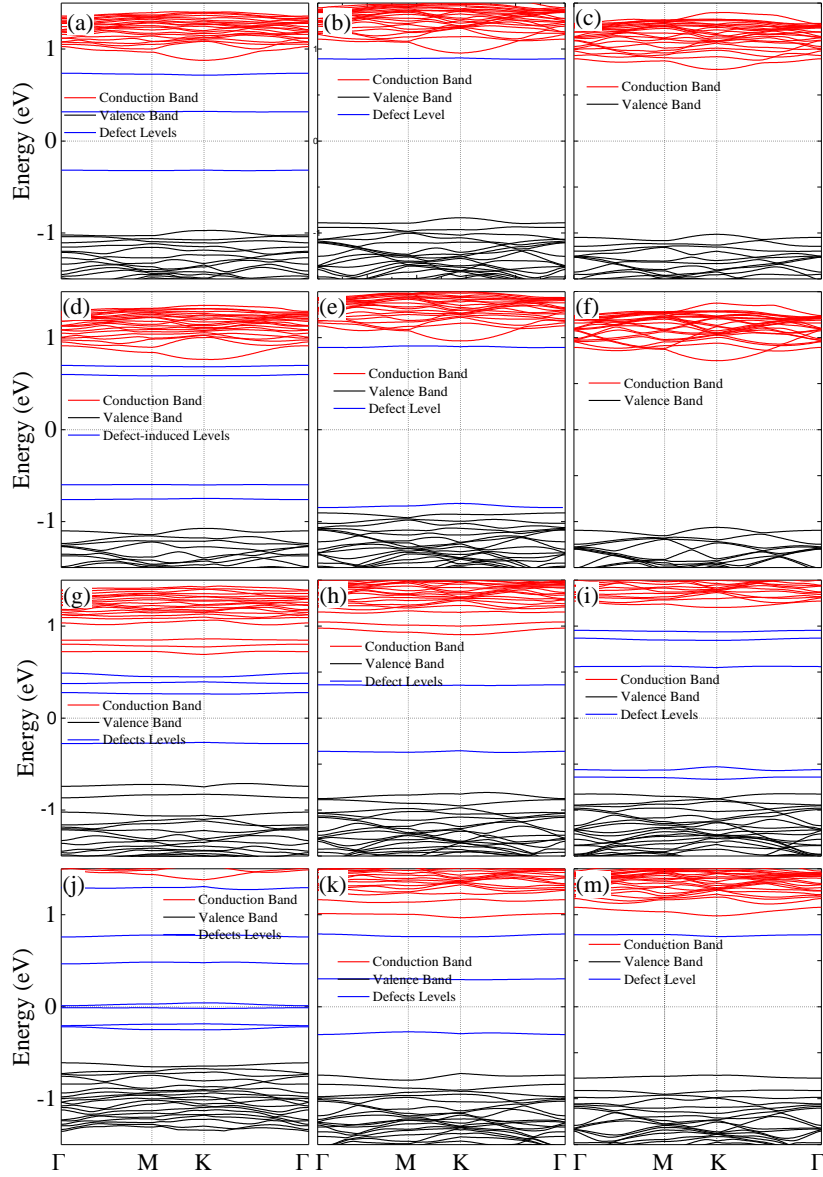


Figure 4. Electronic band structure of MoS₂ monolayer for a 5x5 unit cells with defect of Sulfur shift of (a) $-0.2 \bar{L}_x$ along armchair direction (b) $-0.1 \bar{L}_x$ along armchair direction (c) $0.1 \bar{L}_x$ along armchair direction (d) $0.2 \bar{L}_x$ along armchair direction (e) $0.2 \bar{L}_y$ along zigzag direction (f) $0.1 \bar{L}_y$ along zigzag, and defect of Molybdenum shift of (g) $-0.2 \bar{L}_x$ along armchair direction (h) $-0.1 \bar{L}_x$ along armchair direction (i) $0.1 \bar{L}_x$ along armchair direction (j) $0.2 \bar{L}_x$ along armchair direction (k) $0.2 \bar{L}_y$ along zigzag direction (m) $0.1 \bar{L}_y$ along zigzag direction. The Fermi energy level is aligned to 0 eV.

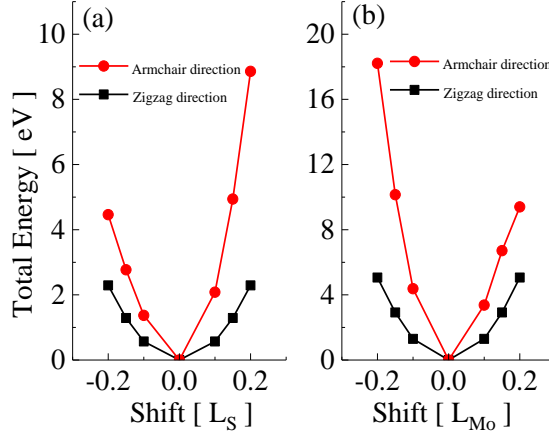


Figure 5. Total energy of 5×5 supercell with (a) S shift vector and (b) Mo shift vector.

In addition, the atomic shift modifies the crystal structural stability as shown in Figure 5. The total energy consists of the exchange-correlation energy, kinetic energy, electrostatic energy, and Mermin free energy, which are explained in detail in the Supplementary Section. The atomic shift of Mo or S along the zigzag direction has better structural stability than the atomic shift along the armchair direction. Also, the total energy for Mo or S atomic shift along the positive and negative zigzag direction has a balanced parabolic energy distribution. However, the total energy for the positive shift of the S atom and the negative shift of the Mo atom along the armchair direction is much higher than that of the negative shift of the S atom and the positive shift of the Mo atom along the armchair direction. It indicates that a single atomic shift in the MoS₂ monolayer forms the characteristic electrostatic energy responding to the ionic charges.

IV. CONCLUSION

The piezoelectric coefficient e_{11} and energy band structure of MoS₂ with 5x5 unit cells were studied as functions of fractional single atomic (Mo or S) shifts to the lattice constant along armchair or zigzag directions. The piezoelectric coefficient e_{11} is for the polarization at the ground state in response to the strain along the armchair direction, where the e_{11} in the D_{3h} point group is related as $e_{11} = -e_{12} = -(1/2)e_{26}$. The analysis found that the piezoelectric coefficient e_{11} was increased up to ~353 pC/m for the +20% atomic shift of Mo along the armchair direction, but it was significantly reduced for the atomic shift of Mo or S atom along the negative armchair direction. The single atomic shifts of Mo and S in the 5x5 unit cells also modified the energy band structure. The single atomic shift also induced new energy levels inside the forbidden bandgap.

Therefore, the pioneering analysis of the piezoelectric coefficient (e_{11}) and energy band structure of 2D atomic layers provides formidable information of the piezoelectric properties and band structure modification in response to a single atomic shift in a MoS₂ monolayer of 5x5 unit cells for the critical and demanding applications of mechano-electric conversion.

ACKNOWLEDGEMENT

This work at HU is supported by ARO W911NF-15-1-0535, NSF HRD-1137747, and NASA NNX15AQ03A.

Reference

1. R. Walczak, J. Dziuban, A.D.T. Elliott, and P.D. Mitcheson, *Procedia Eng.*, 2012, **47**, 1311.
2. S.R. Anton and H.A. Sodano, *Smart Mater. Struct.*, 2007, **16**, R1.
3. Donelan, J. M. et al. *Science*, 2008, **319**, 807–810.
4. R.H. Blick and M. Grifoni, *New J. Phys.*, 2005, **7**, null.
5. S.B. Lakshmanan, X. Zou, M. Hossu, L. Ma, C. Yang, and W. Chen, *J. Biomed. Nanotechnol.*, 2012, **8**, 883.
6. N. Jamond, P. Chrétien, F. Houzé, L. Lu, L. Largeau, O. Maugain, L. Travers, J. C. Harmand, F. Glas, E. Lefeuvre, M Tchernycheva and N. Gogneau, *Nanotechnology*, 2016, **27**, 325403.
7. J. H. Kang, G. Sauti, C. Park, V. I. Yamakov, K. E. Wise, S. E. Lowther, C. C. Fay, S. A. Thibeault and R. G. Bryant, *ACS Nano*, 2015, **9**, 11942–11950.
8. S.-H. Shin, Y.-H. Kim, M.H. Lee, J.-Y. Jung, J.H. Seol, and J. Nah, *ACS Nano*, 2014, **8**, 10844.
9. P. Sun, Y. Liu, X. Wan, X. Meng, R. Su, and S. Yu, *J. Mater. Sci. Mater. Electron.*, 2015, **26**, 6787.
10. P. Sun, F. Xue, S. Yu, X. Meng, Y. Liu, and L. Zhang, *Nanosci. Nanotechnol. Lett.*, 2014, **6**, 927.
11. P. Sun, Y. Li, X. Meng, S. Yu, Y. Liu, F. Liu, and Z. Wang, *J. Mater. Sci. Mater. Electron.*, 2014, **25**, 2974.
12. Z.L. Wang and J. Song, *Science*, 2006, **312**, 242.
13. M.-P. Lu, J. Song, M.-Y. Lu, M.-T. Chen, Y. Gao, L.-J. Chen, and Z.L. Wang, *Nano Lett.*, 2009, **9**, 1223.
14. Y. Li, S. Yu, X. Meng, Y. Liu, Y. Zhao, F. qi Liu, and Z. Wang, *J. Phys. Appl. Phys.*, 2013, **46**, 215101.
15. Y.H. Liu, X.Q. Meng, S. Yu, F. Xue, and X. Wan, *Opt. Spectrosc.*, 2014, **116**, 91.
16. H. Yuan, G. Cheng, S. Yu, A.R.H. Walker, C.A. Richter, M. Pan, and Q. Li, *Appl. Phys. Lett.*, 2006, **108**, 103505.
17. S. Yu, H.D. Xiong, K. Eshun, H. Yuan, and Q. Li, *Appl. Surf. Sci.*, 2015, **325**, 27.
18. S. Yu, H. Zhu, K. Eshun, C. Shi, M. Zeng, and Q. Li, *Appl. Phys. Lett.*, 2016, **108**, 191901.
19. K. Eshun, H.D. Xiong, S. Yu, and Q. Li, *Solid-State Electron.*, 2015, **106**, 44.
20. S. Yu, Q. Li, and K. Eshun, *ECS Trans.*, 2014, **64**, 25.
21. K.-A.N. Duerloo, M.T. Ong, and E.J. Reed, *J. Phys. Chem. Lett.*, 2012, **3**, 2871.

22. S. Bertolazzi, J. Brivio, and A. Kis, *ACS Nano*, 2011, **5**, 9703.
23. J.-H. Lee, J. Y. Park, E. B. Cho, T. Y. Kim, S. A. Han, T.-H. Kim, Y. Liu, S. K. Kim, C. J. Roh, H.-J. Yoon, H. Ryu, W. Seung, J. S. Lee, J. Lee and S.-W. Kim, *Adv. Mater.*, 2017, 1606667
24. L. M. Malard, T. V. Alencar, A. P. M. Barboza, K. F. Mak and A. M. de Paula, *Phys. Rev. B*, 2013, 87, 201401.
25. S. Yu, K. Eshun, H. Zhu, and Q. Li, *Sci. Rep.*, 2015, **5**, 12854.
26. W. Wu, L. Wang, Y. Li, F. Zhang, L. Lin, S. Niu, D. Chenet, X. Zhang, Y. Hao, T.F. Heinz, J. Hone, and Z.L. Wang, *Nature*, 2014, **514**, 470.
27. J. Qi, Y.-W. Lan, A.Z. Stieg, J.-H. Chen, Y.-L. Zhong, L.-J. Li, C.-D. Chen, Y. Zhang, and K.L. Wang, *Nat. Commun.*, 2015, **6**, 7430.
28. S. Manzeli, A. Allain, A. Ghadimi and A. Kis, *Nano Lett.*, 2015, **15**, 5330–5335.
29. M.-Y. Tsai, A. Tarasov, Z. R. Hesabi, H. Taghinejad, P. M. Campbell, C. A. Joiner, A. Adibi and E. M. Vogel, *ACS Appl. Mater. Interfaces*, 2015, **7**, 12850–12855.
30. J. F. Nye, *Physical Properties of Crystals: Their Representation by Tensors and Matrices*, Clarendon Press, 1985.
31. M. Brandbyge, J.-L. Mozos, P. Ordejón, J. Taylor, and K. Stokbro, *Phys. Rev. B*, 2002, **65**, 165401.
32. W. Kohn and L.J. Sham, *Phys. Rev.*, 1965, **140**, A1133.
33. J.P. Perdew, K. Burke, and M. Ernzerhof, *Phys. Rev. Lett.*, 1996, **77**, 3865.
34. S. Grimme, *J. Chem. Phys.*, 2006, **124**, 34108.
35. M.J. Grote and C. Kirsch, *J. Comput. Phys.*, 2004, **201**, 630.
36. H. Zhu, Y. Wang, J. Xiao et al., *Nat. Nanotechnol.*, 2015, **10**, 151–155.
37. R.D. King-Smith and D. Vanderbilt, *Phys. Rev. B*, 1993, **47**, 1651.
38. M. Meyer, S. Glaus and G. Calzaferri, *J. Chem. Educ.*, 2003, **80**, 1221.
39. H.-P. Komsa and A. V. Krasheninnikov, *Phys. Rev. B*, 2015, **91**, 125304.
40. S. KC, R. C. Longo, R. Addou, R. M. Wallace and K. Cho, *Nanotechnology*, 2014, **25**, 375703.